THE ASTROPHYSICAL JOURNAL, 374:266–280, 1991 June 10

MODEL LIGHT CURVES OF LINEAR TYPE II SUPERNOVAE

DOUGLAS A. SWARTZ AND J. CRAIG WHEELER[1]
Department of Astronomy, University of Texas at Austin, Austin, TX 78712
AND
ROBERT P. HARKNESS
University of Texas System Center for High Performance Computing, Austin, TX 78758
Received 1990 June 4; accepted 1990 November 30

ABSTRACT

Light curves computed from hydrodynamic models of supernova explosions are compared graphically with the average observed B and V-band light curves of linear Type II supernovae. Models are based on the following explosion scenarios: carbon deflagration within a C+O core near the Chandrasekhar mass, electron-capture–induced core collapse of an O-Ne-Mg core of the Chandrasekhar mass, and collapse of an Fe core in a massive star. A range of envelope mass, initial radius, and composition is investigated. Only a narrow range of values of these parameters are consistent with observations. Within this narrow range, most of the observed light curve properties can be obtained in part, but none of the models can reproduce the entire light curve shape and absolute magnitude over the full 200 day comparison period. The observed lack of a plateau phase is explained in terms of a combination of small envelope mass and envelope helium enhancement. The final cobalt tail phase of the light curve can be reproduced only if the mass of explosively synthesized radioactive ^{56}Ni is small ($M_{\rm Ni} \sim 0.01\ M_\odot$). The results presented here, in conjunction with the observed homogeneity among individual members of the supernova subclass, argue favorably for the O-Ne-Mg core collapse mechanism as an explanation for linear Type II supernovae. The Crab Nebula may have arisen from such an explosion. Carbon deflagrations may lead to brighter events like SN 1979C.

Subject headings: hydrodynamics — stars: interiors — stars: supernovae

1. INTRODUCTION

Type II supernovae (SN II's) all display Balmer lines in their spectra, but they exhibit a wide range in their photometric properties. Examination of the B light curves of 21 Type II supernovae led Barbon, Ciatti, & Rosino (1979) to identify two clearly distinct subtypes of SN II's: those exhibiting a plateau phase (SN IIP's) and those showing a linear decline (SN IIL's) following maximum light.

Until the recent supernova 1987A, most discussion of supernova light curves en masse ignored the absolute magnitudes of the observations and assumed that individual members within a given class reached the same peak brightness and followed the same morphology (Barbon et al. 1979; Doggett & Branch 1985; however, see also Younger & van den Bergh 1985). SN 1987A in the LMC is one of the dimmest plateau Type II events on record. Matched with the known distance to the LMC, this supernova has clearly illustrated the inherent misrepresentation made by assuming that all events within a given subclass are identical. This has led to a renewed interest in the intrinsic differences between individual members of supernova subtypes, especially their absolute magnitudes, as well as to new attempts to establish the common features (if any) peculiar to each subtype in relation to the others (Young & Branch 1989; Gaskell 1990; Miller & Branch 1990; Tammann & Schröder 1990).

Linear Type II light curves are strikingly similar in peak intrinsic magnitude and overall light curve shape (Young & Branch 1989; Gaskell 1990; Miller & Branch 1990). This is in stark contrast to the large range in these basic characteristics observed among SN IIP events. This homogeneity must, undoubtedly, place stringent constraints on any viable linear Type II model.

In light of these new observational summaries, it is instructive to reevaluate the current theoretical understanding of Type II supernovae. Theoretical models for SN IIP's (Falk & Arnett 1977; Litvinova & Nadyozhin 1983) have enjoyed substantial success in explaining the major features of these supernovae. Most interestingly, the large variation in observed peak luminosity and light curve morphology appears as a natural consequence of the basic SN IIP scenario, where the radius of the progenitor plays a dominant role in the formation of the light curve. On the other hand, except for the preliminary work of Wheeler, Harkness, & Cappellaro (1986), no similar theoretical explanation has been forthcoming describing the nature of SN IIL's. To this end, we present light curves derived from numerical models in an effort to constrain the progenitor characteristics of linear Type II supernovae. Three possible scenarios, together comprising a broad range of parameter space, are considered.

Two scenarios have been suggested in the past to explain linear Type II events. Barbon et al. (1979) outlined the possibility that SN IIL's may be, in most respects, identical to SN IIP's, except that the hydrogen envelope is less massive in SN IIL events. The presence of a short-duration constant-luminosity plateau appears to be a natural extension of the SN IIP scenario when the envelope mass is small (Litvinova & Nadyozhin 1983). Assuming that a stellar wind is responsible for reducing the envelope mass, one expects to observe a continuous range in plateau durations. Barbon et al. (1979) indi-

[1] AURA Visiting Professor, National Optical Astronomy Observatories, which are operated by the Associated Universities for Research in Astronomy, Inc. (AURA), under cooperative agreement with the National Science Foundation.

cate the possibility of one or two transition objects in their sample which have a relatively short plateau period. This suggests that SN IIL's result, as do SN IIP's, from core collapse in a massive star producing a radioactive ^{56}Ni mass of about 0.1 $M_\odot$ to power the late-time tail.

The second scenario is based on the similarity between the light curves of SN IIL and those of Type Ia supernovae. Doggett & Branch (1985) suggested that the same mechanism could be responsible for both supernova subtypes, namely, a thermonuclear explosion in an electron-degenerate C+O core with a mass near the Chandrasekhar limit. In this hypothesis, the main difference between SN IIL's and SN Ia's is the presence or absence, respectively, of an envelope at the time of the explosion. Linear Type II supernovae would then be analogous to the "Type $1\frac{1}{2}$" supernovae described by Iben & Renzini (1983). Such stars are below the mass cut for the development of a nondegenerate C+O core, so they must have a total mass less than about 8 $M_\odot$ at explosion. Bolometric light curves of a model with a 7 $M_\odot$ extended hydrogen envelope (Woosley 1990) look very similar to those of other massive extended envelope supernovae (SN IIP's). Smaller envelope masses are possible, since some fraction of the initial envelope may be lost to pulsations or wind during the growth of the C+O core (Barkat & Tuchman 1980a, b). SN Ia light curves are powered almost exclusively by the radioactive energy release from ^{56}Ni and its daughter nucleus, ^{56}Co, with a negligible contribution from diffusive release of shock energy. Thus, if SN IIL's are indeed similar to SN Ia's, one expects a low-mass, relatively compact progenitor envelope, and a rather bright, cobalt-powered maximum-light display. Such a scenario is particularly favorable for the excessively bright SN 1979C in M100. Young & Branch (1989) have shown that a strong similarity in absolute blue luminosity from peak to 400 days exists between SN 1979C and the Type Ia supernova 1972E.

A third possible scenario for Type II linear supernovae is proposed here. Specifically, we consider core collapse in intermediate-mass stars that have small core masses at the time of explosion. Theoretically, stars in the mass range 8–10 $M_\odot$ will burn carbon nondegenerately, but further evolution toward an iron core is preempted by electron-capture–induced core collapse (Hillebrandt, Nomoto, & Wolff 1984). A considerable amount of dredge-up of the helium mantle occurs prior to collapse, resulting in only a few tenths of a solar mass or less of ejected mantle material. The dredge-up phase leaves the envelope significantly enhanced in helium and CNO-processed nitrogen. The star may also have undergone some mass loss prior to collapse, and a further decrease in the H/He ratio would then be expected (Nomoto et al. 1982). A relatively small amount of explosive nucleosynthesis is likely to occur in such an explosion. This is important for the light curve formation, since the radioactive energy source powering the late-time optical display in Type Ia's and SN IIP's must be formed by nuclear burning during the explosion, and it is likely the same power source drives the late-time light curve of SN IIL's as well. Woosley, Weaver, & Taam (1980) have also modeled the evolution of stars in this mass range and have concluded that the helium mantle and hydrogen envelope will be ejected prior to any collapse phase, in contrast to the conclusions reached by Hillebrandt et al. (1984).

Each of these scenarios is analyzed in the present work. Light curves are derived from hydrodynamic models of stellar explosions. Results are compared graphically with the composite B and V-band photometry of Doggett & Branch (1985). Further details of the observational constraints and a discussion of the computational method are given in the next section. Results from several representative models are presented in § 3. There are arguments in favor of both the hypothesis of Doggett & Branch (1985) of a thermonuclear explosion mechanism and the electron-capture–induced core collapse scenario as valid candidates for producing linear Type II supernovae, although the carbon deflagration models are too bright at late times and the core collapse models decline too rapidly during the linear phase. Further discussion is given in § 4.

2. COMPUTATIONAL METHODS

2.1. *Observational Constraints*

Plateau Type II supernova events maintain a nearly constant luminosity for a period of roughly 80 days past maximum. During this same period, the blue light curve of linear events declines at a constant rate of $\sim$0.05 mag day^{-1}, or 4–5 mag over the entire period. Type Ia supernovae also exhibit a nearly linear decline just after maximum light (Pskovskii 1977, 1984), although the slope is between 0.07 and 0.09 mag day^{-1} (Miller & Branch 1990). The slope of the decline from the end of the plateau phase to the beginning of the final, shallow decline phase (see below) for the plateau Type II events SN 1969L and SN 1987A is also very nearly 0.05 mag day^{-1} (Young & Branch 1989; see also Barbon et al. 1979). This observation is surprising, since theoretical light curves of SN 1987A show that the slope during this period is model-dependent (Woosley 1988; Shigeyama, Nomoto, & Hashimoto 1988).

No bolometric observations of linear Type II supernovae are available. Ten events have been identified as members of the linear subclass on the basis of observations in the B (or photographic) band. Of these, only three events (SN 1970G, SN 1979C, and SN 1980K) have been observed during the entire evolution from maximum light to the final slow decline phase. Five events have been observed in the V band. The resulting composite V-band light curve (Doggett & Branch 1985) is very similar to the composite B-band curve, although at least one exception to this general trend (SN 1980K; Barbon, Ciatti, & Rosino 1982a) shows an abrupt but small change in slope during the linear phase in the V band.

Premaximum data of several SN IIL's indicate that maximum B-magnitude occurs 20–40 days after the explosion and that B increases prior to maximum at a rate of 1–2 mag in about 30 days (Young & Branch 1989). Both SN IIP and SN IIL light curves eventually evolve to a slow decline phase beginning about 100–150 days after maximum and remaining to the limit of observations (in excess of 400 days). Barbon, Cappellaro, & Turatto (1984) have shown that this final portion of the light curve evolves on a time scale consistent with what is expected if the energy source is the radioactive decay of ^{56}Co and the energetic photons released in the decay are all thermalized within the ejecta, but their sample consists of only the anomalously bright SN IIL events SN 1979C and SN 1980K. A similar late-time trend is also observed in the Hα spectral line for the linear Type II SN 1980K (Uomoto & Kirshner 1986). These observations imply that the ejected mass is large enough to trap all the radioactive decay products for at least several hundred days after the explosion. During this final phase, absolute B-magnitude observations recorded in Young

& Branch (1989) show differences of order 2 mag among individual Type II events, although these authors did not correct for reddening in their sample. Such a large difference is not observed in the V band according to Hamuy & Suntzeff (1990).

The peak absolute blue luminosity of SN IIP's spans a large range (Young & Branch 1989), while SN IIL's appear to lie between -16.0 and -18.0 with a mean value of -16.5 (Young & Branch 1989; Miller & Branch 1990; Gaskell 1990). The two most thoroughly observed SN IIL events, SN 1979C (de Vaucouleurs et al. 1981; Barbon et al. 1982b; Panagia et al. 1980) and SN 1980K (Barbon et al. 1982a; Buta 1982), exceed the mean value by 3 mag and 2 mag, respectively. Henceforth, these events are not considered standard linear Type II supernovae, and they are discussed separately.

The sample compiled by Young & Branch (1989) and Gaskell (1990) was not corrected for reddening within the parent galaxy. As the B band is particularly susceptible to reddening, it follows that the derived mean absolute blue magnitude may be underestimated by 0.5 mag or more. There is no reason to assume that the reddening correction will be the same for all events. The real dispersion in peak absolute B-magnitude may be more than reported by Gaskell and by Young & Branch. It is, nevertheless, undeniable that the similarity among linear Type II's is much stronger than that among their SN IIP counterparts, both in intrinsic brightness and in the overall shape of their light curves. This similarity is reminiscent of trends found in Type Ia supernovae. The strong similarity among members of the linear Type II subclass occurs in both the B and V bands throughout the entire temporal range of observation. As a result of this similarity, the composite B and V light curves of Doggett & Branch (1985) will be considered representative of the subclass as a whole and used here for comparison with model results.

There are four main features of the mean observed linear Type II light curve that any viable model must reproduce. These are the 1–2 mag rise to maximum in 20–40 days, a maximum blue luminosity of -16.0 to -18.0, a linear decline at a rate of 0.05 mag day^{-1} for 80–100 days following maximum light, and a final, relatively shallow decline phase roughly parallel to that of the cobalt decay energy release rate. The shape of the composite light curve during the final shallow decline phase is determined by observations of only three events (Young & Branch 1989). Two of these are the bright objects SN 1979C and SN 1980K. The reliability of the composite light curve as a true indication of the mean behavior of SN IIL's at the final phase is therefore questionable.

Statistically, linear Type II supernovae account for only one-tenth (Gaskell 1990) to one-third (Barbon et al. 1979) of all observed Type II events. Type II supernovae occur principally in spiral arms of galaxies, and many are observed in H II regions (with no apparent preference among the subclasses).

There are no clear identifying differences between spectra of Type II supernovae. The most thoroughly observed events, excluding SN 1987A, are the SN IIL events SN 1979C (Panagia et al. 1980; Branch et al. 1981; Barbon et al. 1982b) and SN 1980K (Barbon et al. 1982b; Uomoto & Kirshner 1986). Spectra are nearly Planckian at maximum light, with an effective temperature of about 10^4 K. There is no evidence for an ultraviolet deficit at maximum light as is characteristic of Type Ia and Ib supernovae and as has been observed in at least one SN IIP (SN 1987A). Elemental composition based on spectral diagnostics indicates a nearly solar metallicity for SN IIL's, but the abundance of H and He is uncertain because of limitations in the spectral modeling techniques. Observed photospheric velocities at early times range from 7000 to more than 10,000 km s^{-1}. Late-time spectra of SN II's are characterized by broad emission lines (Kirshner & Kwan 1974, 1975; Branch et al. 1981; Uomoto & Kirshner 1986). Predominant among these is Hα, with significant contributions from once-ionized iron and calcium and neutral oxygen (Kirshner et al. 1973; Branch et al. 1981). The spectrum becomes increasingly non-Planckian as the supernova evolves, but does not necessarily show the strong UV deficit observed in Type Ia spectra and in the plateau Type II SN 1987A. Approximate effective temperatures obtained from late-time spectral scans (Kirshner & Kwan 1974, 1975) are 5000–6000 K. These temperatures are consistent with $(B-V)$ colors (Younger & van den Bergh 1985). SN 1987A also maintains an effective temperature of ~ 5000 K for times in excess of about 20 days, although the U and B bands are below the blackbody flux at least as early as 50 days.

2.2. *Initial Configurations*

Models of linear Type II supernovae based on the three scenarios defined previously encompass at least seven parameters: core mass (M_c), mass of radioactive ^{56}Ni ($M_{\rm Ni}$), explosion mechanism (core collapse or carbon deflagration), kinetic energy imparted to the ejecta ($E_{\rm exp}$), envelope mass ($M_{\rm env}$), envelope extension ($R_{\rm env}$), and envelope composition ($X_{\rm env}$). In an effort to limit the list of potential models, we choose the core mass to remain unchanged within a particular scenario. For example, all massive-star core collapse models assume a 4.2 $M_\odot$ core (1.4 $M_\odot$ neutron star and 2.8 $M_\odot$ ejected mantle). Variations in the envelope mass in any of the models implicitly assumes that the original envelope mass has been diminished, for instance by wind loss. Although such mass loss can have important observational consequences at very late times (Chevalier 1984), accounting for the interaction between the supernova ejecta and any presupernova wind is beyond the scope of the present work. All configurations used here are composed of a core and an overlying envelope. Models of cores and envelopes are constructed individually and then combined to form a complete initial model.

An initial core mass of 1.39 $M_\odot$ is assumed for electron-degenerate O-Ne-Mg core collapse explosions. These cores are constructed using the method described in Sutherland & Wheeler (1984). The composition is assumed to be a homogeneous O-Ne-Mg mixture with mass fractions of 0.2, 0.6, 0.2, respectively, based on the stellar evolution models of Nomoto (1984). The neutron star portion of this core is assumed to have a mass of 1.0 $M_\odot$. The remaining 0.39 $M_\odot$ mantle is ejected in the explosion. This is a relatively large mantle ejecta mass for this configuration, but the results are not sensitive to the precise value.

A similar construction is used to simulate massive core collapse. The original core mass distribution has been kindly provided by A. Marom. In principle, any main-sequence star of mass in excess of 10 or 12 $M_\odot$ can be a candidate for the massive-star progenitor hypothesis of Barbon et al. (1979). The models considered here all have initial core masses of 4.2 $M_\odot$. This value is representative of a main-sequence star of ~ 15 $M_\odot$. The composition of the ejected mantle is approximated from Figure 1 of Woosley & Weaver (1986).

Both core collapse scenarios assume a ^{56}Ni mass of 0.01–0.1 $M_\odot$ uniformly distributed within the inner 0.3 $M_\odot$ of the

mantle. The composition in this region is accordingly modified from the appropriate O-Ne-Mg or massive core mixture.

Model W7 of Nomoto, Thielemann, & Yokoi (1984) is used for the core in simulations of a thermonuclear explosion. This is a model of a white dwarf that has undergone carbon deflagration. The model is representative of the class of objects thought to lead to SN Ia events and has been shown to reproduce the light curve (Nomoto et al. 1984) and near–maximum-light spectra (Harkness 1991) of Type Ia supernovae. The particular model used here has been previously evolved to 3 s after the explosion. All explosive nucleosynthesis has ended by this time, though the material is not yet in homologous expansion. The model has a total mass of 1.38 $M_\odot$, a kinetic energy of 1.3×10^{51} ergs, and a total ^{56}Ni mass of 0.58 $M_\odot$. The elemental composition and the mass and distribution of ^{56}Ni are taken from Thielemann, Nomoto, & Yokoi (1986). The star is totally disrupted, and no neutron star remains.

All envelopes are derived from a single 1.0 $M_\odot$ envelope model consistent with a 2.4 $M_\odot$ red giant star on the Hayashi track. This model has an initial outer radius of 8.5×10^{13} cm. The model was provided by Y. Tuchman. A set of envelopes ranging in mass from 0.1 to 10.0 $M_\odot$ and initial radii from 3.6×10^{12} to 8.5×10^{14} cm are obtained from the 1.0 $M_\odot$ envelope by using a homology transformation. The envelope composition is assumed homogeneous with a solar metallicity. The efficiency of core penetration to enhance the envelope helium abundance is important in low-mass stars. Helium enhancement by this mechanism is believed to occur in both the carbon deflagration (initial main-sequence mass $\lesssim 8$ $M_\odot$) and the electron-capture core collapse (8–10 $M_\odot$) cases. Convective core contraction on the main sequence should also leave the deeper envelope layers of more massive stars helium-enhanced, including the massive-star models represented here. If considerable mass loss then transpires, the final envelope may be considerably helium-enhanced. The degree of helium enhancement is important because the opacity is sensitive to the composition, particularly to the abundance of hydrogen, which in turn affects the light curve. Hydrogen deficiencies up to 50% by mass from the solar value are considered, with the remaining composition assigned to helium. Solar abundances are from Cameron (1982).

Cores and envelopes are merged to form a complete model configuration. Following simulation of an explosion, the evolution of the core is followed until it reaches a radius about 0.01 of the envelope outer radius before merging the core and an envelope. At this stage, the expansion of the core would have swept up only a small fraction of the mass of the envelope, so that no important interaction between the core and envelope could have occurred. If a substantial difference exists between the values of physical quantities at the interface between the outer boundary of the core and the inner boundary of the envelope, a log-linear interpolation of all physical quantities is used to add additional zones within this region. (The envelope is in hydrostatic equilibrium at this stage, and the velocities in the additional zones are assumed to be zero.) Starting from this point, the dynamics of the combined core and envelope are evolved as described below.

Mixing of core and envelope material is not considered. Mixing, most notably of radioactive material into the envelope, is known to affect the early phase of the light curve (Woosley 1988; Shigeyama et al. 1988) and late-time spectrum (Swartz, Harkness, & Wheeler 1989) in models of SN 1987A.

A summary of the initial model configurations is given in Table 1.

TABLE 1

MODEL SUMMARY

Parameter	Carbon Deflagration	Iron Core Collapse	O-Ne-Mg Core Collapse
M_c ($M_\odot$)[a]	1.38	2.80	0.4
M_{Ni} ($M_\odot$)	0.58	0.01–0.1	0.01–0.1
E_{exp} (10^{51} ergs)	1.30	0.5–2.0	0.5–2.0
M_{env} ($M_\odot$)	0.1–3.0	1.0–3.0	1.0–5.0
R_{env} (10^{13} cm)	0.36–85.0	0.36–85.0	0.36–85.0
M_H ($M_\odot$)	0.04–2.31	0.40–2.31	0.40–3.85

[a] Does not include neutron star remnant if any.

2.3. *Numerical Procedure*

Hydrodynamics are followed in spherical symmetry using a standard Lagrangian code with pseudoviscosity (Wheeler & Hansen 1971). Models use 64–172 mass zones for the core and 32–128 zones for the envelope. The number of zones is chosen such that density and composition gradients are thoroughly resolved but such that the zone mass does not vary between adjacent zones by more than an order of magnitude. Accelerations in Rayleigh-Taylor unstable regions are modified using the method discussed in Sutherland & Wheeler (1984). This acceleration tends to smooth the density profile on the 10%–20% level. Rayleigh-Taylor mixing of energy and composition, as discussed in Sutherland & Wheeler, is not included. Nuclear reactions are suppressed.

Shock formation following core collapse is simulated by artificially adding kinetic energy to the material at the inner boundary of the mantle. The kinetic energy is distributed over five mass zones to avoid the formation of a strong shock discontinuity which requires an unacceptably short numerical time step to resolve. The material interior to this point is forced to remain in hydrostatic equilibrium. For numerical purposes, the neutron star matter is retained in the mass grid only as long as the maximum radius of the neutron star material (core) is comparable to the maximum radius of the mantle. After this phase, the model is rezoned with the neutron star core removed. The gravitational force of the neutron star is retained in the equation of motion as an additive constant. A rarefaction wave develops between the core and mantle. In some models this causes a portion of the inner region (less than 0.1 $M_\odot$) of the mantle to fall toward the center of the star, bounce, and move outward again in an oscillatory manner. To prevent this behavior, a minimum velocity of 5×10^7 cm s^{-1} is assigned to the innermost mantle zone. This velocity floor does not alter the total kinetic energy. A floor velocity is unnecessary once the mantle has expanded appreciably.

Simulating thermonuclear explosions is straightforward, since the initial configurations are already evolved to a time past explosive nucleosynthesis.

The energy equation is solved in the equilibrium diffusion approximation (Mihalas & Mihalas 1984, p. 460). The only external energy source is radioactive decay of ^{56}Ni and ^{56}Co. The flux-limiter discussed in Alme & Wilson (1974) is used.

Rosseland mean opacities are calculated assuming LTE excitation-ionization. Mean opacities are pretabulated for each composition as functions of temperature and mass density. Individual tables are required for each change in composition as a function of depth. Sources of opacity include all those listed in Kurucz (1971) and bound-free opacities from heavy metals computed from the photoionization cross sections of Reilman & Manson (1979). Mean opacities are computed from the frequency-dependent opacities over the range 10^{18} to

7×10^{11} Hz, with integration using 40 frequency points per decade.

The diffusion approximation remains valid only in optically thick material. As the supernova ejecta expands, the use of the diffusion approximation becomes increasingly suspect. In particular, the outermost optically thin regions cannot be accurately modeled as the radiation field becomes increasingly anisotropic and non-Planckian. The Rosseland mean opacity underestimates the true line-dominated opacity in these outer regions. To partially offset this shortcoming, the depth-dependent mean opacity used in the energy-balance equation is chosen to be either the maximum of the tabulated mean or 0.05 cm^2 g^{-1} for envelope material or 0.1 cm^2 g^{-1} for the metal-rich core material. These opacity minima are estimates based on opacity contributions not included in the Rosseland mean tables. The most important of these opacity sources arise from nonthermal ionization and resonance line scattering.

Ionization by relativistic electrons dominates the microprocesses associated with cobalt decay heating (Axelrod 1980; Swartz 1989). Thus the LTE ionization used to compute the Rosseland mean tables underestimates the true ionization substantially. For example, the degree of ionization in SN 1987A has been estimated at 10% (McCray 1989), while the plasma temperature is below the recombination temperature for an LTE gas. The opacity above the photosphere due to Thomson scattering alone is therefore of order 0.04 cm^2 g^{-1} for a solar composition. Resonance line opacity is not explicitly included in the opacity tables but is particularly important in metal-rich compositions. Numerical experiments indicate that the inclusion of lines for such compositions enhances the Rosseland mean opacity by up to a factor of 20 for moderate densities and for temperatures in the range 10,000–25,000 K. The minimum opacity used here for the metal-rich core layers is in accord with light-curve computations of Type Ia supernovae (Shurmann 1983 and references therein).

The energy input from radioactive decay of ^{56}Ni and its daughter nucleus, ^{56}Co, is computed using a spherical gray atmosphere program. The detailed γ-ray energy spectrum is ignored, and the material γ-ray opacity is taken to be $\kappa_\gamma = 0.06 Y_e$ cm^2 s^{-1}, following Colgate, Petschek, & Kriese (1980). The Compton scattering opacity is assumed to be purely absorptive, as argued by Sutherland & Wheeler (1984). For the γ-ray deposition problem, the source function is known at the outset and the usual iterative procedure required in the gray atmosphere problem is unnecessary. The gray atmosphere program relies on the current radial grid as established by the hydrocode in order to solve the transfer equations. For this reason, the computation of the γ-ray deposition is postponed until all dynamic effects have subsided and a nearly constant increment radial grid is established (normally characterized by a time $t > 5 \times 10^4$ s). At earlier times, the radioactive heating has no effect on either the dynamics or the luminosity. The γ-ray deposition is computed at 10^4 s intervals for times $t > 5 \times 10^4$ s after the explosion.

The gray atmosphere method has been compared with the approximate method of Sutherland & Wheeler (1984) and found to produce consistent results. The gray atmosphere method is less susceptible to angular integration errors, can be applied to arbitrary radioactive source distributions, and is computationally more expedient than the Sutherland & Wheeler method. Comparison of the Sutherland & Wheeler method to Monte Carlo results is discussed in Ambwani & Sutherland (1988).

The positrons released in the decay of ^{56}Co to ^{56}Fe are assumed to deposit their kinetic energy locally.

2.4. *Light-Curve Computation*

The bolometric magnitude is determined from the luminosity:

$$M_{\rm bol} = -18.793 - 2.5 \log_{10} L_{43} , \quad (1)$$

where L_{43} is the luminosity in units of 10^{43} ergs s^{-1}.

The computation of the material temperature in optically thin regions is suspect in the diffusion approximation (Castor 1972). For this reason we do not allow the material temperature to fall below 1000 K. The "freezing" of matter at this temperature first occurs at the outer boundary and propagates slowly inward. The emergent luminosity is measured either at the surface of the ejecta or at the depth at which the local temperature exceeds the floor temperature by 10%, whichever is deeper. The usual problems of defining the luminosity at a photosphere when the photosphere recedes through the radioactive region are avoided by using the present method. The regions being directly heated by ^{56}Co decay remain hotter than the minimum temperature for times exceeding 50–100 days (depending on the specific model). The luminosity, therefore, is measured at a radius above this region, and the luminosity gradient is necessarily shallow in the neighborhood about this radius, so that the precise depth at which the emergent luminosity is defined is unimportant. At later times, the luminosity equals the instantaneous rate of energy deposition by the radioactive decay products:

$$L = \int_0^R \epsilon(r)\rho(r) d^3 r , \quad (2)$$

where ϵ is the local heating rate in units of energy per unit time and per unit mass, and ρ is the local mass density. The quantity ϵ is the sum of the local integrated γ-ray mean intensity (determined from the gray atmosphere solution) multiplied by the local γ-ray opacity and the local positron deposition rate. The integral is over the entire ejecta volume. By this definition, all the thermalized radioactive decay energy is included in the total luminosity, but none of the escaping γ-ray energy.

Ideally, one would prefer to use equation (1) to compare results with bolometric data, but none are available for linear Type II supernovae. The alternative is to estimate the photon energy distribution, compute B- and V-band light curves from the model emergent flux, and compare these with observed B and V light curves.

Traditionally, theoretical models assume that the photon energy distribution is that of a blackbody with an effective temperature given in terms of the total luminosity and some photospheric radius. This assumption is valid only near maximum light for supernovae, since the spectrum can no longer be represented simply as a blackbody at later times and the position of a photosphere is ill-defined.

A better estimate of the effective temperature at late times can be obtained from observations of SN 1987A. Although this particular supernova is not a member of the linear subclass, it is, nonetheless, a meticulously observed Type II supernova. As such, it should typify many of the important spectral characteristics expected to occur in other hydrogen plasmas under similar conditions. The light curves of SN 1987A, with the possible exclusion of the U band, maintain similar shapes during the period from the decline of the plateau phase to a time in excess of several hundred days (Hamuy et al. 1988).

Many of the spectral features appear to vary only slowly in relative strength during this time, even though the bolometric luminosity is decreasing at least as fast as the cobalt decay time. Similar spectral behavior has been observed for the linear Type II events SN 1979C (Branch et al. 1981) and SN 1980K (Uomoto & Kirshner 1986).

The effective temperature of SN 1987A after about the first month remains nearly constant at a value of 5000 K ± 10%, based on U- to L-band photometry (Catchpole et al. 1987, 1988). Effective temperatures at late times for several other SN IIP events taken from spectral scans also lie in the 5000 K range (Kirshner & Kwan 1974, 1975). These observations are consistent with each other. If the spectral features do not vary significantly in time relative to one another, then the flux emerging in different energy bands remains a constant fraction of the total flux, and a constant energy distribution is analogous to a constant effective temperature.

Based on the above arguments, the effective blackbody temperature used here will be given by an expression which preserves the Planckian photon distribution in terms of the luminosity and photospheric radius at early times but relaxes to the constant value of 5000 K at late times:

$$T_{\rm eff}({\rm K}) = \max\left[\left(\frac{L}{4\pi R_{\rm ph}^2\,\sigma}\right)^{0.25}, 5000\right]. \quad (3)$$

Here, $R_{\rm ph}$ is the photospheric radius, and σ is the Stefan-Boltzmann constant. The photospheric radius is defined as the radius at which the optical depth (computed using the opacities discussed above) reaches unity. Note that this is not necessarily coincident with the depth at which the emergent luminosity is evaluated. The U, B, and V response curves of Azusienis & Straizy (1969) are used to obtain light curves from the blackbody flux defined by the luminosity and effective temperature.

Our use of Planck LTE flux-limited diffusion can lead to errors in the color temperature if the opacity is dominated by electron scattering (Branch 1979, 1987). In that case, the true absorption photosphere lies deeper than the scattering photosphere, and the method used in this work will tend to underestimate the true color temperature. Our method is most reliable during the early recombination phase when there is a steep electron density gradient between the fully ionized optically thick regions and the optically thin outer atmosphere. A frequency-dependent solution including spectral lines is needed for a proper treatment, but this is beyond current capabilities.

An estimate of the ^{56}Ni mass, $M_{\rm Ni}$, can be derived from the above definition of $T_{\rm eff}$ and the observed properties of SN IIL's. At late times, the luminosity equals the instantaneous rate of radioactive energy release (assuming 100% trapping of decay products) and is therefore proportional to $M_{\rm Ni}$:

$$L \sim M_{\rm Ni}\, 6.78 \times 10^9 \exp\left(-\frac{t}{\tau_{\rm Co}}\right) \quad (4)$$

(Sutherland & Wheeler 1984). Here t is the time since the explosion, and $\tau_{\rm Co}$ is the cobalt decay lifetime. The ^{56}Ni mass can be expressed as a function of the absolute B-magnitude using equations (1) and (4), $T_{\rm eff}$ = 5000 K, and the B-band response curve:

$$\frac{M_{\rm Ni}}{M_\odot} = 0.7415 \exp\left(\frac{t}{\tau_{\rm Co}}\right) 10.0^{-0.4 M_B(t) - 7.109}. \quad (5)$$

The observed composite B light curve combined with the mean absolute B-magnitude at maximum light imply $M_B \sim -11.0$ at $t \sim 170$ days. From this value, equation (5) predicts $M_{\rm Ni} \sim 0.01$ $M_\odot$. This can only be a crude estimate, because the time of the explosion is uncertain, only a few observations at late times are available, and the composite sample (three events) includes SN 1980K and SN 1979C. The actual value could easily be several times this prediction. The mass of ^{56}Ni implied by equation (5) for SN 1980K is, for instance, 0.04 $M_\odot$. The assumption of 100% trapping of decay products is made here on the basis of the slope of the composite light curve and may not be true for all linear Type II supernovae.

The computation is terminated at 200 days after the explosion. The light curve is well along its final phase by this time. Data for later times are rare and do not as yet indicate any further interesting developments.

3. RESULTS

The composite B light curves of Doggett & Branch (1985) are used for comparison between model results and observations. For illustrative purposes, observed maximum light is assumed to occur at t = 40 days or at the time of maximum light deduced from the models, and at an absolute value of −17.0 in B. Where additional information can be gained by including a V-band or bolometric model light curve, these are included in the figures accordingly.

3.1. *Carbon Deflagration Models*

Models based on a carbon deflagration explosion retain the least number of free parameters. In addition to the fixed core and ^{56}Ni mass, all carbon deflagration models have explosion energy and ^{56}Ni distribution as given by Nomoto et al. (1984) model W7. Stars in the mass range expected to grow C+O cores under electron-degenerate conditions undergo a dredge-up phase, so that the envelope composition in the carbon deflagration models can be expected to be helium-enhanced. The additional free parameters are the envelope mass and envelope outer radius.

The carbon deflagration model for linear Type II supernovae requires an envelope of relatively small radius and mass in order for the shock heating of the envelope to be of minimal importance to the light curve evolution (as is the case for Type Ia events). Light curves of a model with a 1.0 $M_\odot$ envelope with solar abundances and $R_{\rm env} = 3.6 \times 10^{12}$ cm are shown in Figure 1. The premaximum B light curve is consistent with the observed rise to maximum. The peak B-magnitude is −18.0, or about a factor of 4 brighter than the mean observed value. There is a nearly constant luminosity plateau phase ending at 50 days. This is a real effect of the opacity in the envelope, principally that from Thomson scattering by electrons released in hydrogen ionization. The formation of the nearly constant luminosity plateau phase is attributed to the trapping of radioactive energy by the hydrogen-rich envelope, which delays the release of this energy from the atmosphere. That is, the light curve is already in a cobalt-powered phase at least as early as maximum light, and the plateau is not a result of a slow release of shock-deposited energy. Accordingly the peak brightness does not increase or decrease substantially as the envelope radius is varied (compare the core collapse models discussed below). The excessive brightness at maximum light is a serious failure of the model because there is no physical justification for expecting a much smaller ^{56}Ni mass to be produced in a carbon deflagration. The ^{56}Ni mass needed in this model to

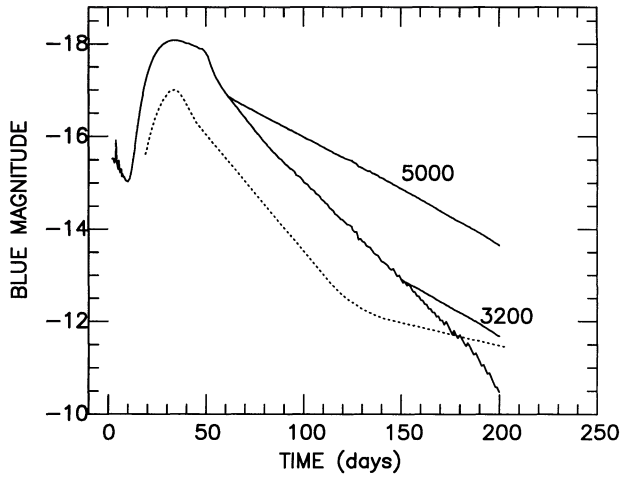

FIG. 1.—Absolute *B*-band light curve of a carbon deflagration model ($M_c = 1.4\ M_\odot$ and $M_{Ni} = 0.58\ M_\odot$) with a $1.0\ M_\odot$ solar abundance envelope and $R_{env} = 3.6 \times 10^{12}$ cm is compared with the composite SN IIL *B* light curve (*dotted line*) of Doggett & Branch (1985) for the first 200 days. Labels denote the value of the minimum allowable effective temperature defined as in eq. (3). The composite light curve is normalized in such a way that the composite and computed *B* maxima coincide in time. For this and for subsequent figures, the composite light curve is assumed to have $M_B = -17.0$ at maximum light.

reduce the peak luminosity by 1.5 mag is $M_{Ni} \sim 0.15\ M_\odot$. The plateau produces too broad a peak to be consistent with observations.

Following the brief plateau phase, the *B* light curve declines at a rate of 0.045 mag day^{-1} and thus follows very closely the requisite 0.05 mag day^{-1} decline. This is the most favorable aspect of the carbon deflagration model. Three versions of the computed *B* light curves are presented in Figure 1 to illustrate the effect of forcing the effective temperature to lie above a fixed value at late times (see eq. [3]). Restricting the effective temperature in this way simply means that a constant fraction of the total available flux, as given by the bolometric light curve, must appear in the various photometric bands. Here, and for other carbon deflagration models to be discussed below, the resulting change in the shape of the light curve arises because of a change in the nature of the spectrum instead of, for instance, a change in the nature of the energy source. Assuming that the effective temperature is given in terms of the luminosity and the position of the photosphere at all times produces a *B* light curve which remains in the linear phase and never turns onto a more shallow "cobalt tail" phase. Requiring the effective temperature to be not less than 5000 K forces the linear phase to terminate prematurely, with the subsequent cobalt tail beginning too soon and at a much brighter level than the observed tail. This is attributable to the large mass of radioactive material which maintains a high luminosity. The slope of the cobalt tail is steeper than the observed slope because the small total ejecta mass in this model fails to trap efficiently the high-energy photons emitted in ^{56}Co decay. Thus, under either definition of the effective temperature, this carbon deflagration model fails to reproduce the late-time light curve behavior. This result is representative of all otherwise viable carbon deflagration models. A *B* light curve with minimum $T_{eff} = 3200$ K is also included in Figure 1 to illustrate that the onset of the late-time tail in this model can be forced to coincide with the observed mean light curve behavior by adjusting the minimum value of T_{eff}. There is no physical justification for such a low value of T_{eff}.

The $1.0\ M_\odot$ solar abundance envelope model is too bright at maximum and produces a recognizable plateau. A smaller mass envelope produces a shorter duration plateau. The envelope mass cannot, however, be much less than $1.0\ M_\odot$ for the standard SN IIL. In the limit $M_{env} \to 0$, the light curve approaches that of a Type Ia (Fig. 2) and becomes even brighter, peaks too early, and declines more steeply than the observed SN IIL light curve. If the envelope mass is increased to $3.0\ M_\odot$, the trapping of radioactive decay energy is enhanced and a broader peak results (Fig. 2). The light curve tends toward a nearly constant luminosity plateau-like character for a period of order 50 days past maximum or $\sim$80 days past initial outburst. A massive envelope expands relatively slowly, which increases the effective trapping of radioactive decay energy and establishes a steady display around maximum light. A larger mass envelope has the advantage of producing a dimmer maximum-light display, but the constant-luminosity plateau is incompatible with the observations. There is not a carbon deflagration model with an envelope of solar composition which produces a peak luminosity consistent with the mean observed value, $M_B = -16.5$, while not producing a flat plateau phase.

The principal limitation of solar abundance models is the persistence of a constant-luminosity plateau phase. If the composition is altered by reducing the mass fraction of hydrogen and increasing that of helium (higher mass number elements remaining unchanged), then the opacity is lower and the constant-luminosity plateau is suppressed. Light curves from models with hydrogen depletions of 0.5 solar and $M_{env} = 1$ and $3\ M_\odot$ are shown in Figure 3. The light curve does not exhibit the characteristic constant-luminosity plateau phase, although the peak is still too broad for $M_{env} \gtrsim 1\ M_\odot$. Helium is less opaque than hydrogen at all times. The trapping of decay energy is less effective in a helium-dominated plasma than in a hydrogen-dominated plasma, and this energy is radiated at an earlier time than in a comparable model with a solar abundance envelope. The resulting maximum light occurs

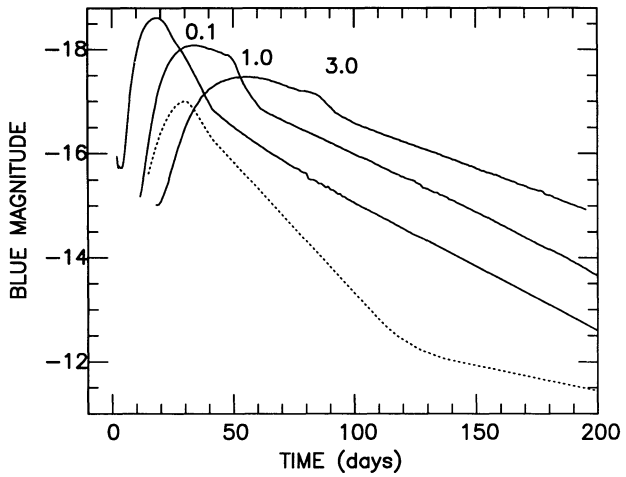

FIG. 2.—Absolute *B*-band light curves of carbon deflagration models with envelopes of solar abundance, $R_{env} = 3.6 \times 10^{12}$ cm, and various masses are compared with the composite *B* light curve. Labels denote envelope mass in solar mass units. For this and for succeeding figures, unless otherwise noted, the minimum allowable effective temperature is 5000 K (see eq. [3]).

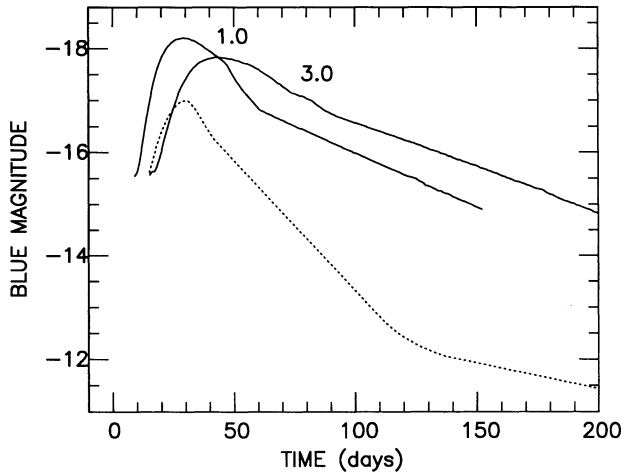

FIG. 3.—Absolute *B*-band light curves of carbon deflagration models with helium-enhanced envelopes, $R_{env} = 3.6 \times 10^{12}$ cm, and various envelope masses are compared with the composite *B* light curve. Labels denote envelope mass in solar mass units. The envelope composition has a 50% reduction in hydrogen by mass from the solar value: $X = 0.5X_{\odot}$, $Y = Y_{\odot} + 0.5X_{\odot}$, $Z = Z_{\odot}$.

earlier and is brighter than for solar abundance models. Enhancing the helium at the expense of hydrogen permits a larger envelope mass to be consistent with the observed lack of a constant-luminosity plateau. The late-time light curves of models differing only in envelope composition are identical because the envelope has recombined, become transparent, and no longer affects the light curve (compare Figs. 1 and 3). Helium-enhanced envelope carbon deflagration models must be compact in order to prevent excessive brightness at maximum light for the same reasons as for solar models.

In summary, carbon deflagration models are characterized by light curves that are dominated by the radioactive decay of ^{56}Ni and ^{56}Co. The 1.0 $M_{\odot}$ envelope helium-enhanced model best reproduces the shape of the observed light curve from pre–maximum light to the onset of the cobalt tail phase, but is brighter than the mean observed light curve at maximum by $\sim$1.5 mag. It is also too bright during the cobalt tail phase. The contrast between the peak and the onset of the cobalt tail is only 1.5 mag in *B*, while the observed contrast is 4–5 mag. The contrast in the models can be increased by increasing the contribution of shock energy during the maximum light phase (by increasing the initial radius), but the carbon deflagration models are already too bright even with a compact envelope because of the large radioactive energy input. In addition, the slope of the late-time tail is too steep. If the sparse late-time observations are taken at face value, these are the two most serious objections to the deflagration models because they rely on the slope of the light curve and the relative differences in brightness, and not on absolute values.

3.2. *Massive-Star Core Collapse Models*

As with the carbon deflagration models, a broad range of envelope masses, initial radii, and helium enhancements are theoretically plausible in massive-star core collapse models. In addition, the explosion energy and the ^{56}Ni mass are variable parameters because the amount of kinetic energy imparted to the ejecta and the extent of nucleosynthesis following collapse of the core are uncertain. The kinetic energy is expected to lie within the range (0.5–2.0) $\times$ 10^{51} ergs and the ^{56}Ni mass in the range 0.01–0.1 $M_{\odot}$. There are five free parameters for massive-star core collapse models: M_{Ni}, M_{env}, R_{env}, X_{env}, and E_{exp}.

For extended hydrogen-rich envelopes, the duration of the plateau phase is shortened as the envelope mass is decreased. This result was illustrated by Litvinova & Nadyozhin (1983), among others, and constitutes the support of the idea put forth by Barbon et al. (1979) that SN IIL's merely have smaller mass hydrogen envelopes than those of SN IIP's at the time of explosion. Compact envelope massive-star models produce light curves that rise slowly to maximum light and are considerably dimmer at maximum light compared with extended envelope models. Compact models do not exhibit a constant-luminosity plateau phase. For compact models, the peak phase is driven, as in the case of Type Ia and the compact linear Type II carbon deflagration models, by cobalt decay, with the shock energy contribution to the total luminosity being negligible. Such features have been discussed previously in relation to models for SN 1987A (Woosley 1988) and do not resemble SN IIL's. The expected configuration for a linear Type II supernova arising from a massive-star core collapse consists, therefore, of a moderately low mass but extended envelope.

Light curves of models all with a 1.0 $M_{\odot}$ hydrogen envelope, $M_{Ni} = 0.1$ $M_{\odot}$, $E_{exp} = 1.0 \times 10^{51}$ ergs, but various initial envelope radii are shown in Figure 4. The most compact model light curve shows an initial decline followed by a rise to a cobalt-powered maximum. If this "secondary peak" is correlated with the observed composite maximum, then the maximum brightness is too dim by $\sim$1 mag, indicating that there is an insufficient mass of radioactive material to exclusively power the observed maximum-light display. An extended envelope is necessary to reproduce the observed SN IIL light curve *shape* near maximum light for core collapse models because the secondary peak is not observed, but, at the large value of the initial radius needed to prevent formation of a secondary peak, the light curve at maximum is brighter than the observed mean value by nearly 2 mag. The optimal radius deduced from fitting the maximum-light *B*-magnitude is $R_{env} \sim 2.5 \times 10^{13}$ cm, although this model shows a secondary peak.

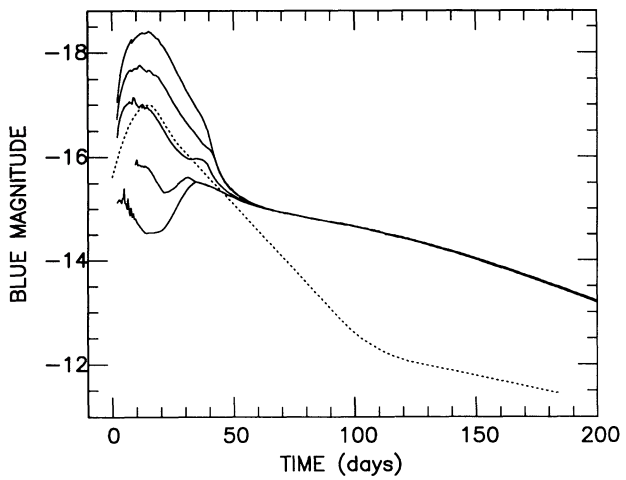

FIG. 4.—Absolute *B*-band light curves of massive-star core collapse models ($M_c = 4.2$ $M_{\odot}$ including a 1.4 $M_{\odot}$ neutron star) with a 1.0 $M_{\odot}$ solar abundance envelope and various envelope radii are compared with the composite *B* light curve. All models have $M_{Ni} = 0.1$ $M_{\odot}$. The envelope radii are *top to bottom*): 8.5×10^{13}, 5.1×10^{13}, 2.5×10^{13}, 8.5×10^{12}, and 3.6×10^{12} cm.

Increasing the envelope mass produces light curves displaying features similar to those displayed in Figure 4, except that the secondary peak will occur at a later time and the plateau phase is flatter. Compare, for example, the SN 1987A models of Woosley (1988). The envelope mass must be of the order of $M_{env} \sim 1\ M_\odot$ if the envelope composition is solar and the ^{56}Ni mass is $\sim 0.1\ M_\odot$. The initial envelope radius and the envelope mass are not totally independent variables. The effects caused by variations of these parameters also occur if the explosion energy is varied instead. An increase in the total energy corresponds to an increase in the internal energy. For a fixed envelope mass, this increase in internal energy gives rise to an increase in the peak luminosity and is equivalent to an increase in envelope extension. Theoretically, the initial envelope radius may vary over several decades, but the explosion energy is most likely to remain in the range of (0.5–2.0) $\times 10^{51}$ ergs. The range in variation of the light curve correlated with changes in explosion energy within these limits is negligible compared with the range of variation associated with allowed changes in the envelope radius. Similarly, the variation in the light curve caused by changing the envelope mass is much more noticeable than the variation related to changes in the explosion energy within this restricted range. The only variations in the light curves caused by increasing the explosion energy are that the luminosity at maximum light increases and the time to maximum light decreases. At late times, the more energetic explosions lead to a greater transparency to γ-rays. The light curve reflects this transparency in a steeper late-time decline. There are no restrictions (within the theoretical bounds) on the explosion energy parameter based on models considered here.

If the mass of radioactive material is decreased from the fiducial value of 0.1 $M_\odot$, the secondary peak will be dimmer, so that it will not be as readily discernible as the envelope radius is decreased. This trend is illustrated in Figure 5 for the $R_{env} = 2.5 \times 10^{13}$ cm model shown in Figure 4 and for a similar model but with a 3 $M_\odot$ envelope in Figure 6. The light curve at maximum light is unchanged as expected, since it is dominated by shock energy release. The slope of the cobalt tail is also unchanged, although the brightness decreases with decreasing

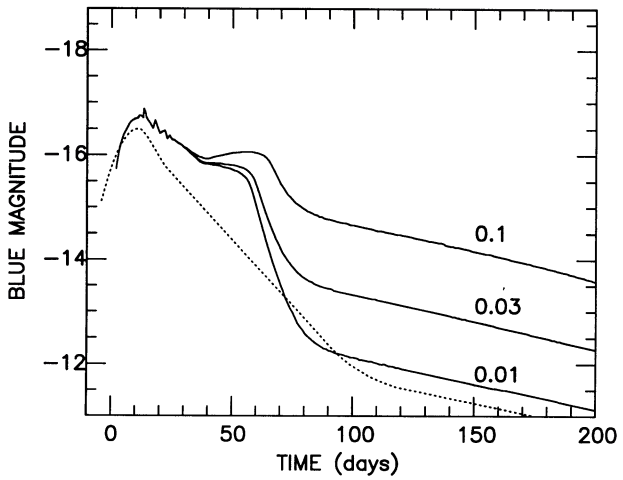

FIG. 6.—Absolute B-band light curves of massive-star collapse models with a 3.0 $M_\odot$ solar abundance envelope, $R_{env} = 2.5 \times 10^{13}$ cm, and various ^{56}Ni abundances are compared with the composite B light curve. Labels denote the initial ^{56}Ni mass in solar mass units.

^{56}Ni mass in accord with equation (5). Figure 7 shows that decreasing the ^{56}Ni mass and the initial envelope radius simultaneously improves the fit to both the maximum-light and the late-time mean absolute B brightness, while suppressing the appearance of a secondary peak. In addition, once the secondary peak is sufficiently suppressed by decreasing the ^{56}Ni content, a larger envelope mass must be retained to maintain the proper slope during the linear phase. The best fit to the observed absolute B light curve during the cobalt-powered tail phase is provided by $M_{Ni} \sim 0.01\ M_\odot$. For this ^{56}Ni mass, the optimum envelope mass is $\sim 3\ M_\odot$.

The linear phase of the B light curve following maximum light and preceding the cobalt tail consists of two portions in all the massive-star core collapse models presented so far. This is a general feature of the core collapse models. During the first portion, the envelope is optically thick and the light curve is powered by the slow release of shock-deposited energy, although the small envelope mass prevents a *constant-*

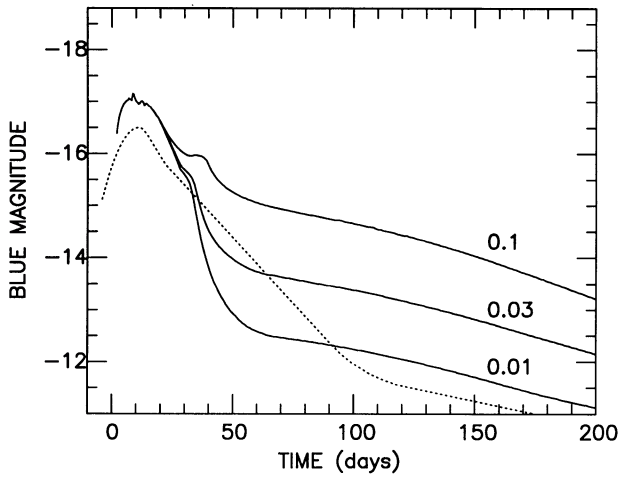

FIG. 5.—Absolute B-band light curves of massive-star core collapse models with a 1.0 $M_\odot$ solar abundance envelope, $R_{env} = 2.5 \times 10^{13}$ cm, and various ^{56}Ni abundances are compared with the composite B light curve. Labels denote the initial ^{56}Ni mass in solar mass units.

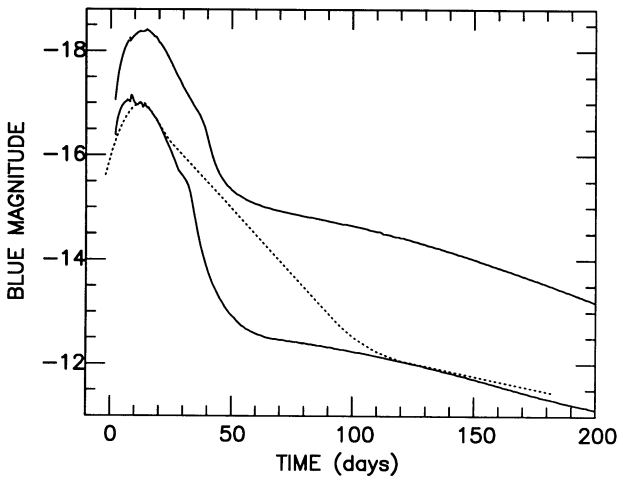

FIG. 7.—Absolute B-band light curves of a massive-star core collapse model with a 1.0 $M_\odot$ solar abundance envelope, $R_{env} = 8.5 \times 10^{13}$ cm, and $M_{Ni} = 0.1\ M_\odot$ (*top*), and a similar model but with $R_{env} = 2.5 \times 10^{13}$ cm and $M_{Ni} = 0.01\ M_\odot$ (*bottom*), are compared with the composite light curve. Note the strong similarity in light curve shapes.

luminosity plateau phase; indeed, the slope during the "plateau" or envelope recombination phase closely matches the observed mean *linear* phase. In contrast to the carbon deflagration models, the peak display is powered by shock energy and the small ^{56}Ni mass is insufficient to replenish the energy loss from the envelope. The result is a decrease in luminosity during the plateau phase which correlates with the linear phase of the observed light curve. The transition to a transparent envelope corresponds to the beginning of the second portion of the linear phase. This kink in the linear-phase light curve is not discernible in the observed composite *B* or *V* light curves but may be seen in the *V*-band light curve of SN 1980K (Barbon et al. 1982a). In the models, the kink is related to the composition contrast between the envelope and the mantle. The mantle is less opaque than the hydrogen-rich envelope, so that, once the envelope becomes transparent, the mantle is already transparent and the light curve declines rapidly to approximately the level of instantaneous cobalt energy deposition. (For carbon deflagration models there is a constant luminosity during the plateau phase, and the linear decline is correlated with the period of envelope transparency. The difference in slope of this later stage and the corresponding stage of the massive-star model is due to the larger amount of energy input from radioactive decay in the deflagration models, which maintains a higher temperature and hence a larger optical depth.) It is important to view this result in the context of the numerical limitations of the models because it is within optically thin regions that the validity of the diffusion approximation and the representation of the opacity by a Rosseland mean are most uncertain.

The contrast between the peak and the onset of the cobalt tail phase in the *B* band is determined by the initial envelope radius and the mass of ^{56}Ni. Since both these quantities are free parameters of the core collapse models, the observed contrast of ~ 5 mag can be reproduced. The mass of ^{56}Ni required to produce a 5 mag contrast while maintaining the observed mean *B* at maximum is $\sim 0.01\ M_\odot$. The rate of decline during the cobalt tail phase is parallel to the observed rate, suggesting that the larger total ejecta mass ($M \gtrsim 4\ M_\odot$) of these massive star models is favored over the smaller mass carbon deflagration models, which do not trap all of the cobalt decay products. The onset of the cobalt tail phase does not correlate with the onset of the effective temperature minimum, as was the case for the deflagration models, although the tail is brighter, since the minimum effective temperature is forced to remain above 5000 K.

Envelope helium enhancement tends to steepen the light curve during the plateau phase and to suppress the contrast in the light curve slope between the plateau phase and the phase prior to the onset of the cobalt tail. Both these effects are attributable to the lower opacity of ionized helium compared with ionized hydrogen. This allows a larger mass envelope to be present while remaining consistent with the observed light curve shape because the increase in slope due to helium enhancement during the plateau phase is offset by the decrease in slope normally occurring when the envelope mass is increased. Figure 8 illustrates results for massive-star models with different envelope and ^{56}Ni masses, $R_{\rm env} = 2.5 \times 10^{13}$ cm, and a 50% reduction by mass of hydrogen from the solar value. Again, the 1.0 $M_\odot$ envelope model becomes too steep during the linear phase if $M_{\rm Ni} < 0.1\ M_\odot$. The slope is steeper than for the corresponding solar abundance model. The slope during the linear phase is better represented by the 3 $M_\odot$ envelope

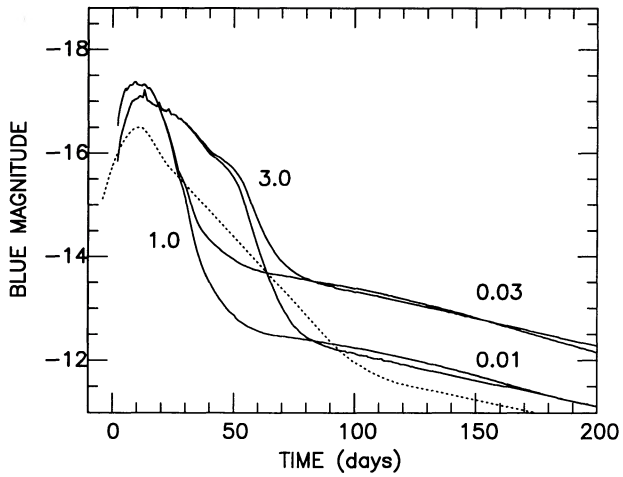

FIG. 8.—Absolute *B*-band light curves of massive-star core collapse models with 1.0 and 3.0 $M_\odot$ helium-enhanced envelopes, $R_{\rm env} = 2.5 \times 10^{13}$ cm, and various ^{56}Ni masses are compared with the composite *B* light curve. Labels on the left-hand side denote the envelope mass in solar mass units, and labels at the right denote the ^{56}Ni mass. The envelope composition is as in Fig. 3.

model, but the light curve is still too broad at maximum light. An abrupt change in slope during the linear phase is not evident unless the ^{56}Ni mass is smaller than $\sim 0.1\ M_\odot$. The optimal values of $M_{\rm Ni}$ and $M_{\rm env}$ are 0.01 and 3.0 $M_\odot$, respectively, for helium-enhanced massive-star core collapse models. Once the envelope becomes transparent, the light curve of helium-enhanced models is identical to those of the solar abundance models as illustrated in Figure 9. The effect of helium enhancement in massive-star core collapse models is not as striking as in the carbon deflagration models because the envelope constitutes a smaller fraction of the total ejecta mass. The composition of at most 20% of the mass of the ejecta is affected by changing the envelope hydrogen abundance in models with a 3.0 $M_\odot$ envelope.

The massive-star core collapse model most representative of the observed light curve (Fig. 9) has a 3.0 $M_\odot$ helium-enhanced envelope (1.15 $M_\odot$ of hydrogen) with initial radius $R_{\rm env} = 2.5$

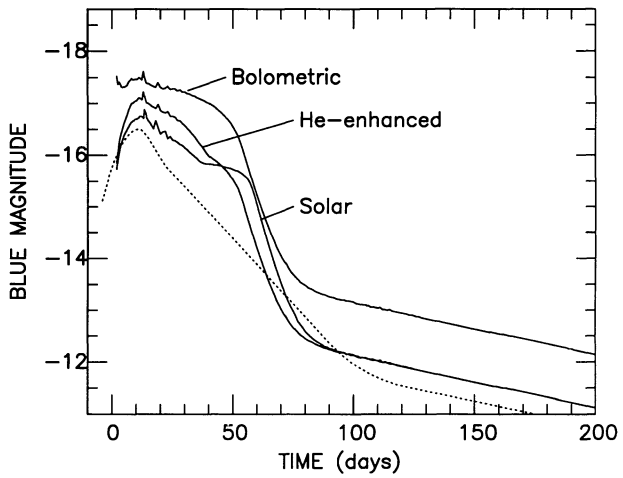

FIG. 9.—Absolute *B*-band light curves of massive-star collapse models with a 3.0 $M_\odot$ envelope, $R_{\rm env} = 2.5 \times 10^{13}$ cm, $M_{\rm Ni} = 0.01\ M_\odot$ and different envelope elemental compositions are compared with the composite *B* light curve. The bolometric light curve of the helium-enhanced model is also included. The envelope composition of the helium-enhanced model is as in Fig. 3.

$\times 10^{13}$ cm and $M_{Ni} = 0.01\ M_\odot$. This model has $M_B = -17.0$ at maximum light and reproduces the observed peak luminosity, although the light curve near maximum light is broader than observed. In accord with observations, there is no discernible constant-luminosity plateau phase. The linear portion of the light curve corresponds to the period of envelope recombination. Following this phase, the light curve falls more steeply than observed before turning onto the cobalt tail. The transition to the late-time cobalt tail is evident in the light curve and is attributable to the change in power source from shock-deposited energy to cobalt decay energy, and not to forcing the effective temperature to remain above the minimum value, a feature in contrast to the carbon deflagration models. The B-band light curve during the cobalt tail phase is of the proper slope, suggesting that larger total ejecta masses are favored (because of better γ-ray trapping). The small initial ^{56}Ni mass ($M_{Ni} \sim 0.01\ M_\odot$) is required to reproduce the absolute magnitude along the tail.

In summary, the fundamental difference between the core collapse and the carbon deflagration scenario is the importance of shock heating to the near–maximum-light display and the allowed variability in the ^{56}Ni mass. A judicious combination of initial envelope radius and ^{56}Ni mass can therefore be made which provides the proper brightness at maximum light and the requisite contrast of 5 mag between the peak and the onset of the cobalt tail phase. The maximum-light and linear portions of the model light curve are powered by the diffusive release of shock energy. As a result, the core collapse models are very sensitive to the initial envelope radius, and this quantity must be roughly 2.5×10^{13} cm, depending only moderately on the envelope composition and the explosion energy. The massive-star core collapse models also require a narrow envelope mass range in order to reproduce the basic observed light curve characteristics. The optimal envelope mass is $\sim 3\ M_\odot$ and is only mildly sensitive to the envelope composition. The models produce a linear phase composed of two sections because of the opacity contrast between the core and the envelope.

Theoretically, the massive-star scenario encompasses a large range of initial stellar configurations. It is difficult to reconcile this fact with the restrictive parameter range deduced here or with the observed homogeneity among the various members of the linear Type II subclass. This makes massive-star core collapse models unlikely candidates for producing linear Type II supernovae.

3.3. *Electron-Capture–induced Core Collapse Models*

The fundamental difference between the massive-star core collapse models and those representing core collapse in O-Ne-Mg cores is the mass of the mantle ejected. Only a few tenths of a solar mass of mantle material is ejected in electron-capture core collapse, while several solar masses are ejected in an Fe core collapse. This difference leads to differences in the final mass distribution (Fig. 10) which may be important to the spectrum as well as to the light curve. Both classes of models produce only a small amount of ^{56}Ni in the explosion, so that the light curves near maximum light in both cases are dominated by the diffusive release of shock energy instead of by radioactive decay, and the cobalt tails are considerably dimmer than for carbon deflagration models. The dependence of the light curve shape on the initial envelope radius for the O-Ne-Mg core models is similar to the dependence found for massive-star core collapse models because of the dominance of

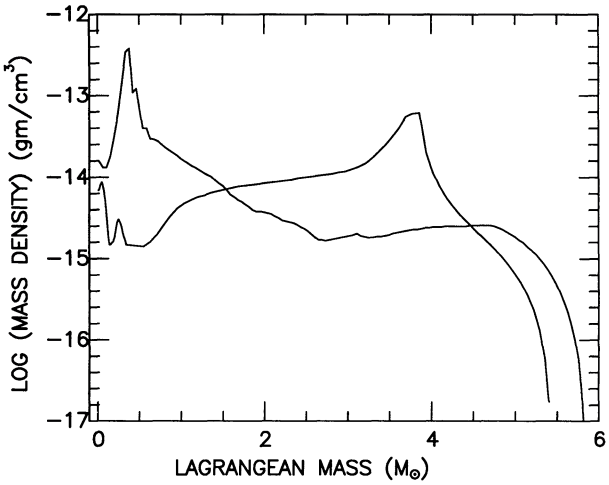

FIG. 10.—Logarithm of the final mass density of a massive-star core collapse model and an O-Ne-Mg core collapse model are shown plotted against the Lagrangian mass coordinate of the ejecta. The massive-star model has a 3.0 $M_\odot$ envelope, an initial core mass of $M_c = 4.2\ M_\odot$ (1.4 $M_\odot$ neutron star), and a total ejecta mass of 5.8 $M_\odot$. The O-Ne-Mg model has a 5.0 $M_\odot$ envelope, an initial core mass of $M_c = 1.4\ M_\odot$ (1.0 $M_\odot$ neutron star), and a total ejecta mass of 5.4 $M_\odot$. The neutron stars are not included in the figure. Both models began with an initial radius of $R_{env} = 8.5 \times 10^{13}$ cm.

shock heating to the near–maximum-light curve. One can anticipate that the small mantle mass ejected in O-Ne-Mg core collapse will permit a larger envelope mass to be retained than for massive-star models and still remain within the observed light curve constraints. The effects of envelope composition should be important for the present set of models in contrast to the massive-star models, because the envelope mass constitutes a major fraction of the total ejecta mass. The most important parameters to be investigated for electron-capture core collapse models are, therefore, the envelope mass, M_{env}, and the envelope composition, X_{env}.

Light curves for a model with a helium-enriched composition (hydrogen reduced to 50% of the solar value) 3.0 $M_\odot$ envelope, $R_{env} = 2.5 \times 10^{13}$ cm, $E_{exp} = 1.0 \times 10^{51}$ ergs, and $M_{Ni} = 0.1$, 0.03, and 0.01 $M_\odot$ are shown in Figure 11. The peak

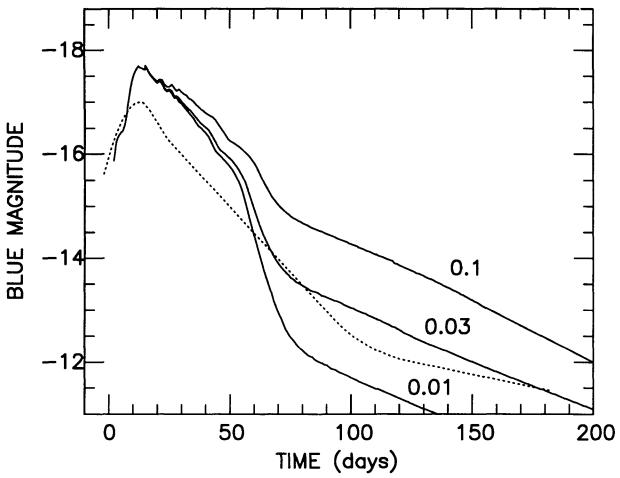

FIG. 11.—Absolute B-band light curves of O-Ne-Mg core collapse models ($M_c = 1.4\ M_\odot$ including a 1.0 $M_\odot$ neutron star remnant) with a 3.0 $M_\odot$ helium-enhanced envelope, $R_{env} = 2.5 \times 10^{13}$ cm, and various ^{56}Ni masses are compared with the composite B light curve. Labels denote initial ^{56}Ni masses in solar mass units. The envelope composition is as in Fig. 3.

B-magnitude is -17.6 and occurs at 12 days. The light curve near maximum light is of roughly the observed shape, but the brightness in the B band at maximum is higher than results from the best massive-star core collapse model. The premaximum slope is steeper than the mean curve. The agreement near maximum light lasts well into the linear phase; however, the linear phase of the light curve is composed of two portions, as was the case for the massive-star models. Once the envelope becomes transparent, the light curve drops rapidly to the cobalt tail phase. The transition to the cobalt tail phase in the models occurs earlier than observed, but the decline in the B light curve from the peak to the onset of the cobalt tail is roughly the observed value of 5 mag if the ^{56}Ni mass is 0.01 $M_\odot$. The cobalt tail is of the correct strength for this model but slightly steeper than the observed curve. The light curve produced by the O-Ne-Mg core collapse model is very similar in structure to the light curve produced by massive core collapse models.

The dependence of the light curve on the envelope mass is similar to that found for the massive-star core collapse models. A comparison of the light curves for the 3 $M_\odot$ envelope model with 0.01 $M_\odot$ of ^{56}Ni from Figure 11, and a similar model but with a 5 $M_\odot$ envelope, is presented in Figure 12. As the envelope mass is increased, the slope during the first portion of the linear phase decreases, while the duration of this portion of the light curve increases. The slope during the linear phase is best reproduced by the model with a 3.0 $M_\odot$ envelope, although the 5.0 $M_\odot$ envelope model is not unreasonable. These light curves are brighter than the mean light curve at maximum brightness. A more compact envelope would decrease the peak luminosity but would also tend to broaden the peak of the light curve and decrease the postpeak slope.

As discussed in terms of the massive-star core collapse models (Fig. 7), the combination of envelope radius and ^{56}Ni mass can be adjusted to produce similar light curve shapes, but with different absolute magnitudes. This trend is shown in Figure 13 using the 5 $M_\odot$ envelope model with $R_{env} = 2.5 \times 10^{13}$ cm and $M_{Ni} = 0.01\ M_\odot$ and with $R_{env} = 8.5 \times 10^{13}$ cm and $M_{Ni} = 0.03\ M_\odot$.

In summary, the small mantle mass ejected in O-Ne-Mg core collapse models permits a larger envelope mass to be retained and still remain within the majority of the observed light curve constraints. The envelope mass is ~ 3.0 to ~ 5.0 $M_\odot$. As with the massive-star core collapse models, the peak luminosity is determined by the shock-heating energy source and is proportional to the initial radius. The optimum envelope radius is roughly 2.5×10^{13} cm, although the peak luminosity is 1 mag too bright for the 3 or 5 $M_\odot$ envelope model with this radius.

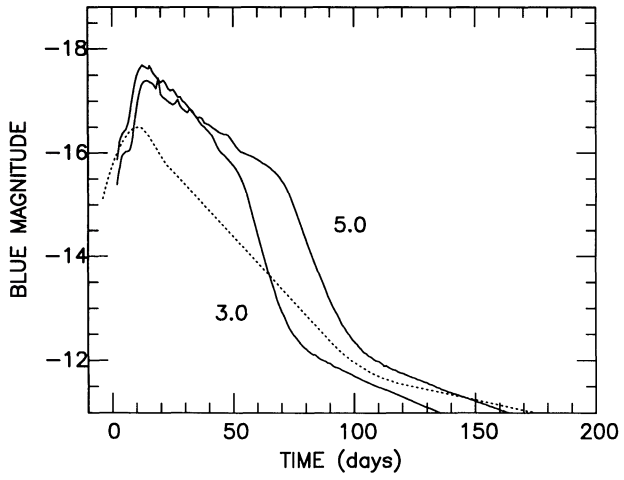

FIG. 12.—Absolute B-band light curves of O-Ne-Mg core collapse models with helium-enhanced envelopes, $R_{env} = 2.5 \times 10^{13}$ cm, $M_{Ni} = 0.01\ M_\odot$, and various envelope masses are compared with the composite B light curve. Labels denote the envelope masses in solar mass units. The envelope composition is as in Fig. 3.

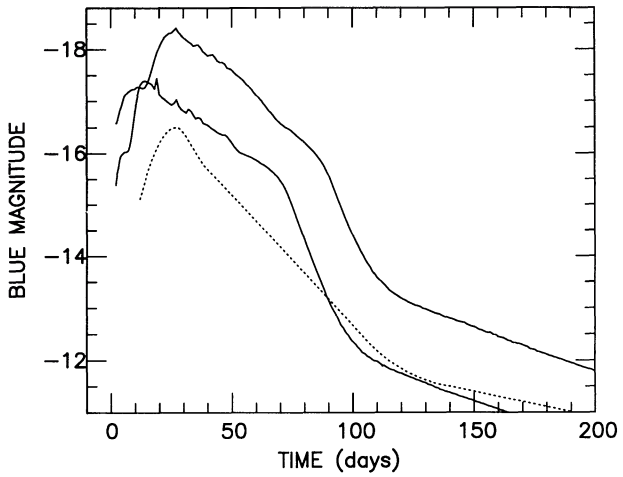

FIG. 13.—Absolute B-band light curves of an O-Ne-Mg core collapse model with a 5.0 $M_\odot$ helium-enhanced envelope, $R_{env} = 8.5 \times 10^{13}$ cm, and $M_{Ni} = 0.03\ M_\odot$ (*top*), and a similar model but with $R_{env} = 2.5 \times 10^{13}$ cm and $M_{Ni} = 0.01\ M_\odot$ (*bottom*), are compared with the composite light curve. Note the strong similarity in light curve shapes. The envelope composition is as in Fig. 3.

The linear phase of the light curve is composed of two portions, as was the case for the massive-star models if the envelope contains solar abundances. A smoother light curve results if the envelope is helium-enhanced, and only these models are acceptable. The best fit to the linear phase is for a model with an envelope mass comparable to or larger than the best fit from the massive-star models. The transition to the cobalt tail phase in the models occurs earlier than observed. The decline in the B light curve from the peak to the onset of the cobalt tail is about 5 mag, and the cobalt tail is of the proper brightness provided $M_{Ni} \sim 0.01\ M_\odot$.

The massive-star and electron-capture core collapse models produce very similar light curves provided that the envelope radius and mass are roughly the same. Electron-capture core collapse models can accommodate a somewhat larger envelope mass than is allowed by core collapse models. A larger envelope mass may be desirable, since hydrogen dominates the observed spectra of linear Type II supernovae even at very late times. Electron-capture–induced core collapse occurs only within a narrow range of initial stellar masses. It is most probable that stars within this mass range evolve along very similar paths. Thus the problem of reconciliation with the observed homogeneity among events discussed in terms of the massive-star models is not encountered here. The electron-capture–induced core collapse models provide the most likely scenario for linear Type II supernovae.

4. CONCLUSIONS

4.1. *General*

Light curves derived from numerical models have been used to constrain the progenitor characteristics of linear Type II

supernovae. Three possible scenarios, together comprising a broad range of parameter space, have been considered. Comparison with the observed average blue light curve has shown that many otherwise plausible models do not represent linear Type II supernovae. For each class of models, only a narrow range of envelope mass and initial radius can be consistent with the observed light curve. A summary of the properties of the best model from each of the three scenarios is given in Table 2. Among those models showing reasonable agreement with observations, there remain important discrepancies which prevent selection of one particular model as being thoroughly representative of the linear subclass of Type II supernovae.

A few conclusions of a general nature are apparent from the present study. The observed relative difference between the B-magnitude at maximum light and at the onset of the cobalt tail cannot be achieved by models whose light curves are powered exclusively by radioactive decay of ^{56}Ni and ^{56}Co. Some amount of shock-deposited energy must contribute to the peak display, and this implies that an extended envelope is present. The envelope extension is severely restricted, on the other hand, by the fact that the peak mean absolute blue magnitude is only -16.5. In order to produce the proper peak luminosity and the peak-to-tail contrast, the initial envelope radius must be $R_{\rm env} \sim 2.5 \times 10^{13}$ cm and the initial ^{56}Ni mass must be $M_{\rm Ni} \sim 0.01\ M_\odot$. This combination rules out carbon deflagration models, in general, as unrepresentative of the mean properties of linear Type II supernovae.

The envelope mass must be small, ranging from 1 to 5 $M_\odot$ for core collapse models and from 0.5 to 1 $M_\odot$ for carbon deflagration models, in order to produce the observed light curve shape near maximum (including the width of the peak and the postpeak slope). This conclusion in itself is not surprising, since the duration of the plateau phase is roughly proportional to the envelope mass, but must favor the electron-capture–induced core collapse models because of their narrow initial mass range. As has been shown in this work, helium enhancement improves the fit to the observations while at the same time allowing a larger envelope mass to be retained. In particular, helium enhancement provides a better fit to the slope during the linear phase of the light curves in core collapse models and helps to remove the constant-luminosity plateau occurring in carbon deflagration models. The effect is most prominent for the O-Ne-Mg core collapse models where the envelope constitutes a significant fraction of the total ejecta mass. A natural means of achieving substantial helium enhancement is known from stellar evolution calculations either through the helium gradient left behind during convective core contraction on the main sequence or dredge-up of core material by the convective envelope in the red giant or supergiant phase, so that helium enrichment of the envelopes of linear Type II supernovae is plausible in view of the moderate ejecta mass required. This implies, in addition, the prior ejection of some outer hydrogen-rich envelope material which exposes the helium-rich layers.

TABLE 2

MODEL RESULTS

Parameter	Carbon Deflagration	Iron Core Collapse	O-Ne-Mg Core Collapse
$M_{\rm Ni}\ (M_\odot)$	0.58	0.01	0.01
$E_{\rm exp}\ (10^{51}$ ergs)	1.30	1.00	1.00
$M_{\rm env}\ (M_\odot)$	<1.0	3.00	3.00
$M_{\rm H}\ (M_\odot)$	<0.4	1.15	1.15
$R_{\rm env}\ (10^{13}$ cm)	0.36	2.50	2.50
$t_{\rm peak}$ (days)	29	11	12
$M_B^{\rm peak}$	-18.2	-17.1	-17.6
Postpeak slope (mag day^{-1})	0.045	0.041	0.053

Except at the very earliest times, helium enhancement cannot be deduced from spectral observations in the visual or UV wavelength bands. The He I 10830 Å line is, however, expected to be strong throughout at least the first several hundred days of the lifetime of the supernova. Observations of linear Type II supernovae at near-infrared wavelengths could help establish the abundance and stratification of helium in the ejecta. (Incidentally, such observations are needed for all supernovae, since the helium abundance has not been well established for any supernova type.) At least one supernova remnant, namely, the Crab Nebula, is known to be significantly enhanced in helium (MacAlpine et al. 1989). As indicated by Nomoto et al. (1982), electron-capture core collapse is a likely scenario for the Crab supernova event, based on this helium enhancement in the absence of a carbon enhancement. If this is the case, then it is likely, too, that the Crab supernova was a linear Type II supernova.

The linear phase of the light curve of core collapse models consists of two portions distinguished by a change in slope. The envelope is in a stage of recombination and is optically thick during the first portion, and the envelope is transparent during the second portion. The change in slope of the light curve between the two portions correlates with the transition to envelope transparency. The resulting light curve fails to match the observed composite B light curve in this detail because the composite has a constant slope throughout the linear phase. The best core collapse model light curves reproduce the mean linear phase slope during the first portion but are too steep during the second portion. The difference in slope between the two portions can be reduced either by increasing the envelope helium abundance or by mixing of the envelope and mantle material. Either of these solutions reduces simply to reducing the contrast in the material opacity of the mantle with that of the envelope. An increase in the mass of hydrogen will not reduce this difference in slope. An increase in the mass fraction of hydrogen (assuming also a mixing of material) would require a decrease in the total ejecta mass to maintain the proper linear phase slope.

The two-portion linear phase does not appear to be a general feature of linear Type II supernova. There is one supernova, SN 1980K, showing such a feature in the V band, although this particular supernova is not representative of the linear subclass as a whole, since it is a factor of 6 brighter than the mean at maximum light. Thus, additional photometry of linear Type II supernovae is needed to establish whether the light curve of SN 1980K is peculiar in these regards or not. Additional observations at wavelengths other than in the B and V bands would be helpful in this analysis. Ideally, a complete set of spectrophotometry would be of tremendous benefit not only to the establishing of a more complete data base but also to the alleviation of one of the greatest uncertainties in the numerical results, namely, the need to convert from bolometric results to color systems. Additionally, there is a scarcity of observational data at late times. The slope and absolute magnitude of the mean B light curve during the cobalt tail is determined by only three events, and two of these are clearly unrepresentative of the mean at maximum light. Based on the

available information, and pending future observations, the mass of radioactive material created in linear Type II supernova explosions must be very small, and the core collapse scenario must be favored.

4.2. *SN 1979C*

The current comparison of models with observations has focused on the mean light curve normalized to the mean absolute magnitude of -16.5. What has not been emphasized is that the most thoroughly observed linear Type II supernovae, SN 1979C and SN 1980K, are brighter than this mean by ~ 3 and 2 mag, respectively. The distance and reddening to SN 1980K are uncertain, although this is not the case for SN 1979C. These supernovae demand additional comment.

All the models presented here are too dim at maximum light in comparison with SN 1979C. As the trends of the models have indicated, the initial envelope radius for the core collapse models must be very large if SN 1979C results from such an explosion, and the envelope mass must be very small and strongly helium-enhanced if this supernova is a carbon deflagration event. The latter scenario can also be made consistent with the late-time light curve by the following argument. The only late-time light curve data available for SN 1979C are for times in excess of 250 days after maximum light. The lack of data between 100 and 250 days after the explosion prevents an accurate determination of the slope of the late-time light curve of SN 1979C. It is possible, therefore, that the actual slope is much steeper than that of the mean SN IIL curve. If this is the case, then significant γ-ray escape has occurred, and the amount of radioactive material cannot be deduced from the late-time light curve. For SN 1979C it is possible that a much larger ^{56}Ni mass is present but that γ-ray transparency reduces the light curve to the level of the mean observed curve at late times. This is consistent with a carbon deflagration scenario for SN 1979C with a small total mass. If this is the case, SN 1979C and the other linear Type II supernovae might be closely related, but the former comes from a star of $M < 8\ M_\odot$, while the latter come from stars of slightly larger mass (Wheeler 1990). Such a carbon deflagration model is compared with the observed B and V light curves of SN 1979C in Figure 14. The observational data are from the B and V data tabulated in Barbon et al. (1982b) and de Vaucouleurs et al. (1981), and the distance modulus is taken from Miller & Branch (1990). The observations are normalized in time in such a way that the observed and computed B maxima coincide. The model has an initial radius of 8.5×10^{13} cm, an envelope mass of $1.0\ M_\odot$, and a hydrogen depletion of 50% of solar. For this particular model, the minimum effective temperature (eq. [3]) is set to 4200 K to improve the fit to the late-time observations. This lower value of $T_{\rm eff}$ forces a lower flux both in B and in V. The slope during the final phase is unaffected by the choice of the minimum effective temperature. The model is slightly dimmer than the observed curve at maximum and would be ~ 0.5 mag brighter than the observations along the final decline phase if $T_{\rm eff}^{\rm min} = 5000$ K. The model light curve is broader at maximum light than the observed composite light curve, and the apparently good fit to the SN 1979C data during this phase might be a fortuitous consequence of the lack of pre–maximum-light observations for this event.

It is, therefore, possible that SN 1979C exploded by carbon deflagration instead of by core collapse. The basic light curve is then similar to the standard SN IIL curve despite the difference in the total ^{56}Ni ejected, and hence the absolute luminosity at maximum and the shape of the late-time tail. If there are different mechanisms, then spectral modeling near maximum light and at late times should reveal significant differences and provide further clues to the origins of these events.

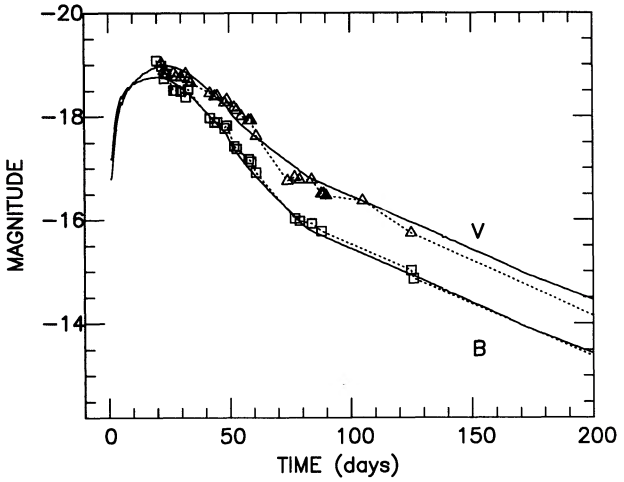

FIG. 14.—V and B light curves of a carbon deflagration model are compared with the observed light curves of SN 1979C. The observed V data are indicated by triangles, and the B-band data by squares. The data are from Barbon et al. (1982b) and de Vaucouleurs et al. (1981), using the distance modulus from Miller & Branch (1990). Additional data for times later than 200 days exist, and the late-time observed light curves (*dotted lines*) are defined by those points even though they are not shown in the figure. The observations are normalized in such a way that the observed and computed B maxima coincide in time. No adjustment of the absolute magnitudes has been made. The model has the following parameters: $R_{\rm env} = 8.5 \times 10^{13}$ cm, $M_{\rm env} = 1.0\ M_\odot$, and a hydrogen depletion of 50% of solar (the latter as in Fig. 3). For this particular model, the minimum effective temperature (eq. [3]) is set to 4200 K to improve the fit to the late-time observations.

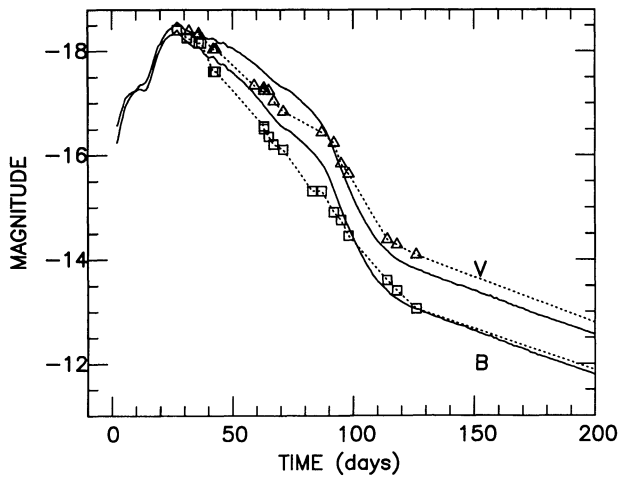

FIG. 15.—V and B light curves of an O-Ne-Mg core collapse model are compared with the observed light curves of SN 1980K. The observed V data are indicated by triangles, and the B-band data by squares. The data are from Barbon et al. (1982a), using the distance modulus from Miller & Branch (1990). Additional data for times later than 200 days exist, and the late-time observed light curves (*dotted lines*) are defined by those points even though they are not shown in the figure. The observations are normalized in such a way that the observed and computed B maxima coincide in time. No adjustment of the absolute magnitudes has been made. The model has the following parameters: $R_{\rm env} = 8.5 \times 10^{13}$ cm, $M_{\rm env} = 5.0\ M_\odot$, $M_{\rm Ni} = 0.03\ M_\odot$, and a hydrogen depletion of 50% of solar (the latter as in Fig. 3). No adjustment of the minimum effective temperature from the fiducial value of 5000 K (eq. [3]) has been made for this model.

4.3. *SN 1980K*

The peak blue magnitude of SN 1980K is -18.5 (using the distance modulus given by Miller & Branch 1990). This supernova is 2 mag brighter than the mean. The peak-to-tail contrast is 5 mag, and the slope of the light curve during this linear phase is 0.05 mag day^{-1} in *B*. Both these properties are in agreement with the mean composite light curve properties. The ^{56}Ni mass implied by the observations, assuming $T_{\rm eff} = 5000$ K at late times, is $\sim 0.03\ M_\odot$. Figure 15 compares the *B* and *V* light curves of SN 1980K to those from an O-Ne-Mg model with the following parameters: $M_{\rm env} = 5\ M_\odot$, $R_{\rm env} = 8.5 \times 10^{13}$ cm, $M_{\rm Ni} = 0.03\ M_\odot$, and a hydrogen depletion of 50% of solar (see Fig. 12). The observational data are from the *B* and *V* data tabulated in Barbon et al. (1982a), and the distance modulus is taken from Miller & Branch (1990). The observations are normalized in time in such a way that the observed and computed *B* maxima coincide. Although this model is unrepresentative of the *mean* linear Type II behavior (principally because it is too bright at maximum light), it does illustrate the possibility that the precisely linear slope indicated by the composite light curves requires further observational confirmation.

4.4. *Summary*

The observed homogeneity among members of the linear subclass of Type II supernovae requires a restricted range of the initial envelope radius, mass, and composition and the amount of ^{56}Ni produced if the models are to reproduce the observations. The homogeneous nature of the majority of SN IIL's seems to be best explained by models in a restricted initial mass range which undergo helium enhancement of their envelopes by core penetration and dredge-up, form a degenerate O-Ne-Mg core, and collapse to trigger the explosion. If this is the correct explanation, then some wind-type mass loss must have reduced the initial envelope mass, but a catastrophic envelope ejection to form a planetary nebula must not have occurred. The light curves provide constraints on the evolution which must lead to this narrow range of envelope mass, radius, and composition. The Crab Nebula supernova may have been of this class. Immediate progenitors may be identified with the *s*-processed and lithium-enhanced asymptotic giant branch stars in the LMC and the SMC which have $M_{\rm bol} = -7.1$, corresponding to Chandrasekhar mass cores (Wheeler 1990). SN 1979C, with its significantly higher peak luminosity, may be based on a deflagration.

This work was supported in part by the R. A. Welch Foundation and by NSF grant 8717166. The computations were done on the Cray X-MP of the University of Texas System Center for High Performance Computing. We are grateful to Ken Nomoto for helpful discussion.

REFERENCES

Alme, M. L., & Wilson, J. R. 1974, ApJ, 194, 147
Ambwani, K., & Sutherland, P. G. 1988, ApJ, 325, 820
Axelrod, T. S. 1980, Ph.D. thesis, Univ. Calif. Santa Cruz
Azusienis, A., & Straizy, V. 1969, Soviet Astr., 13, 316
Barbon, R., Cappellaro, E., & Turatto, M. 1984, A&A, 135, 27
Barbon, R., Ciatti, F., & Rosino, L. 1979, A&A, 72, 287
———. 1982a, A&A, 116, 35
Barbon, R., Ciatti, F., Rosino, L., Ortolani, S., & Rafanelli, P. 1982b, A&A, 116, 43
Barkat, Z., & Tuchman, Y. 1980a, ApJ, 237, 105
———. 1980b, ApJ, 242, 199
Branch, D. 1979, MNRAS, 186, 609
———. 1987, ApJ, 320, L23
Branch, D., Falk, S. W., McCall, M. L., Rybski, P., Uomoto, A. K., & Wills, B. J. 1981, ApJ, 244, 780
Buta, R. J. 1982, PASP, 94, 578
Cameron, A. G. W. 1982, in Essays in Nuclear Astrophysics, ed. C. A. Barnes, D. D. Clayton, & D. N. Schramm (Cambridge: Cambridge Univ. Press), 23
Castor, J. 1972, ApJ, 178, 779
Catchpole, R. M., et al. 1987, MNRAS, 229, 15P
Catchpole, R. M., et al. 1988, MNRAS, 231, 75P
Chevalier, R. A. 1984, Ann. NY Acad. Sci., 422, 215
Colgate, S. A., Petschek, A. G., & Kriese, J. T. 1980, ApJ, 237, L81
de Vaucouleurs, G., de Vaucouleurs, A., Buta, R., Ables, H. D., & Hewitt, A. V. 1981, PASP, 93, 36
Doggett, J. B., & Branch, D. 1985, AJ, 90, 2303
Falk, S. W., & Arnett, W. D. 1977, ApJS, 33, 515
Gaskell, M. 1990, preprint
Hamuy, M., & Suntzeff, N. B. 1990, AJ, 99, 1146
Hamuy, M., Suntzeff, N. B., Gonzalez, R., & Martin, G. 1988, AJ, 95, 63
Harkness, R. P. 1991, in Supernovae, ed. S. E. Woosley (New York: Springer-Verlag), 454
Hillebrandt, W., Nomoto, K., & Wolff, R. G. 1984, A&A, 133, 175
Iben, I. I., & Renzini, A. 1983, ARA&A, 21, 271
Kirshner, R. P., & Kwan, J. 1974, ApJ, 193, 27
———. 1975, ApJ, 197, 415
Kirshner, R. P., Oke, J. B., Penston, M. V., & Searle, L. 1973, ApJ, 185, 303
Kurucz, R. 1971, SAO Spec. Rept., No. 309 (Cambridge: SAO)
Litvinova, I. Yu., & Nadyozhin, D. K. 1983, Ap&SS, 89, 89
MacAlpine, G. M., McGaugh, S. S., Mazzarella, J. M., & Uomoto, A. 1989, ApJ, 342, 364
McCray, R. 1989, in Molecular Processes in Astrophysics, ed. T. H. Hartquist (Cambridge: Cambridge Univ. Press), 231
Mihalas, D., & Mihalas, B. W. 1984, Foundations of Radiation Hydrodynamics (Oxford: Oxford Univ. Press)
Miller, D. L., & Branch, D. 1990, AJ, 100, 530
Nomoto, K. 1984, ApJ, 277, 791
Nomoto, K., Sparks, W. M., Fesen, R. A., Gull, T. R., Miyaji, S., & Sugimoto, D. 1982, Nature, 299, 803
Nomoto, K., Thielemann, F.-K., & Yokoi, K. 1984, ApJ, 286, 644
Panagia, N., et al. 1980, MNRAS, 192, 861
Pskovskii, Yu. P. 1977, Soviet Astr., 21, 675
———. 1984, Soviet Astr., 28, 688
Reilman, R. F., & Manson, S. T. 1979, ApJS, 40, 815
Schurmann, S. R. 1983, ApJ, 267, 779
Shigeyama, T., Nomoto, K., & Hashimoto, M. 1988, A&A, 196, 141
Sutherland, P. G., & Wheeler, J. C. 1984, ApJ, 280, 282
Swartz, D. A. 1989, Ph.D. thesis, Univ. Texas
Swartz, D. A., Harkness, R. P., & Wheeler, J. C. 1989, Nature, 337, 439
Tammann, G. A., & Schröder, A. 1990, A&A, 236, 249
Thielemann, F.-K., Nomoto, K., & Yokoi, K. 1986, A&A, 158, 17
Uomoto, A., & Kirshner, R. P. 1986, ApJ, 308, 685
Wheeler, J. C. 1990, in Supernovae, ed. J. C. Wheeler, T. Piran, & S. Weinberg (Singapore: World Scientific), 1
Wheeler, J. C., & Hansen, C. J. 1971, Ap&SS, 11, 373
Wheeler, J. C., Harkness, R. P., & Cappellaro, E. 1986, in Proc. 13th Texas Symposium on Relativistic Astrophysics, ed. M. P. Ulmer (Singapore: World Scientific), 402
Woosley, S. E. 1988, ApJ, 330, 218
———. 1990, in Supernovae, ed. A. G. Petschek (Berlin: Springer-Verlag), 182
Woosley, S. E., & Weaver, T. A. 1986, ARA&A, 24, 205
Woosley, S. E., Weaver, T. A., & Taam, R. E. 1980, in Proc. Texas Workshop on Type I Supernovae, ed. J. C. Wheeler (Austin: Univ. Texas Press), 113
Young, T. R., & Branch, D. 1989, ApJ, 342, L55
Younger, P. F., & van den Bergh, S. 1985, A&AS, 61, 365